Supplementary Material (ESI) for the paper

Two isomorphous Co(II) coordination polymers based on new α,α-disubstituted derivatives of zoledronic acid: synthesis, structures and properties

Tomasz Rojek,[a] Waldemar Goldeman,[a] Katarzyna Ślepokura[b], Marek Duczmal[a], Agnieszka Wojciechowska[a] and Ewa Matczak-Jon*[a]

[a] Department of Chemistry, Wrocław University of Science and Technology, Wybrzeże Wyspiańskiego 27, 50-370 Wrocław, Poland. E-mail: ewa.matczak-jon@pwr.edu.pl

[b] Faculty of Chemistry, University of Wrocław, Joliot-Curie 14, 50-383 Wrocław, Poland.

Spectroscopic characterization of compound **1** and **2**:

1-hydroxy-2-(1*H*-imidazol-1-yl)-2-methylpropylidene-1,1-diphosphonic acid (compound **1**): ^{1}H NMR (300 MHz, D_2O+NaOD) δ: 1.69 (s, 6H, 2×CH_3), 6.66 (d, $^{3}J_{HH}$ = 0.9 Hz, 1H, imidazole-*H*), 7.19 (d, $^{3}J_{HH}$ = 0.9 Hz, 1H, imidazole-*H*), 7.70 (d, $^{3}J_{HH}$ = 0.9 Hz, 1H, 2-imidazole-*H*); ^{31}P NMR {^{1}H} (121 MHz, D_2O+NaOD) δ: 17.42 (s, 2P); ^{13}C NMR (75 MHz, D_2O+NaOD) δ: 26.78 (*C*H_3), 63.31 (t, $^{2}J_{CP}$ = 5.1 Hz, $(CH_3)_2$*C*), 81.00 (t, $^{1}J_{CP}$ = 125.4 Hz, P-*C*-P), 121.23, 124.38, 138.64.

1-hydroxy-2-[1-(1*H*-imidazol-1-yl)cyclopropyl]ethylidene-1,1-diphosphonic acid (compound **2**): ^{1}H NMR (300 MHz, D_2O+NaOD) δ: 0.64 (m, 2H, CH_2), 1.23 (m, 2H, CH_2), 6.51 (s, 1H, imidazole-*H*), 7.28 (s, 1H, imidazole-*H*), 7.77 (s, 1H, 2-imidazole-*H*); ^{31}P NMR {^{1}H} (121 MHz, D_2O+NaOD) δ: 17.50 (s, 2P); ^{13}C NMR (75 MHz, D_2O+NaOD) δ: 11.60 (t, $^{3}J_{CP}$ = 3.3 Hz, *C*H_2), 40.65 ($(CH_2)_2$*C*), 74.42 (t, $^{1}J_{CP}$ = 127.1 Hz, P-*C*-P), 123.57, 124.71, 141.37.

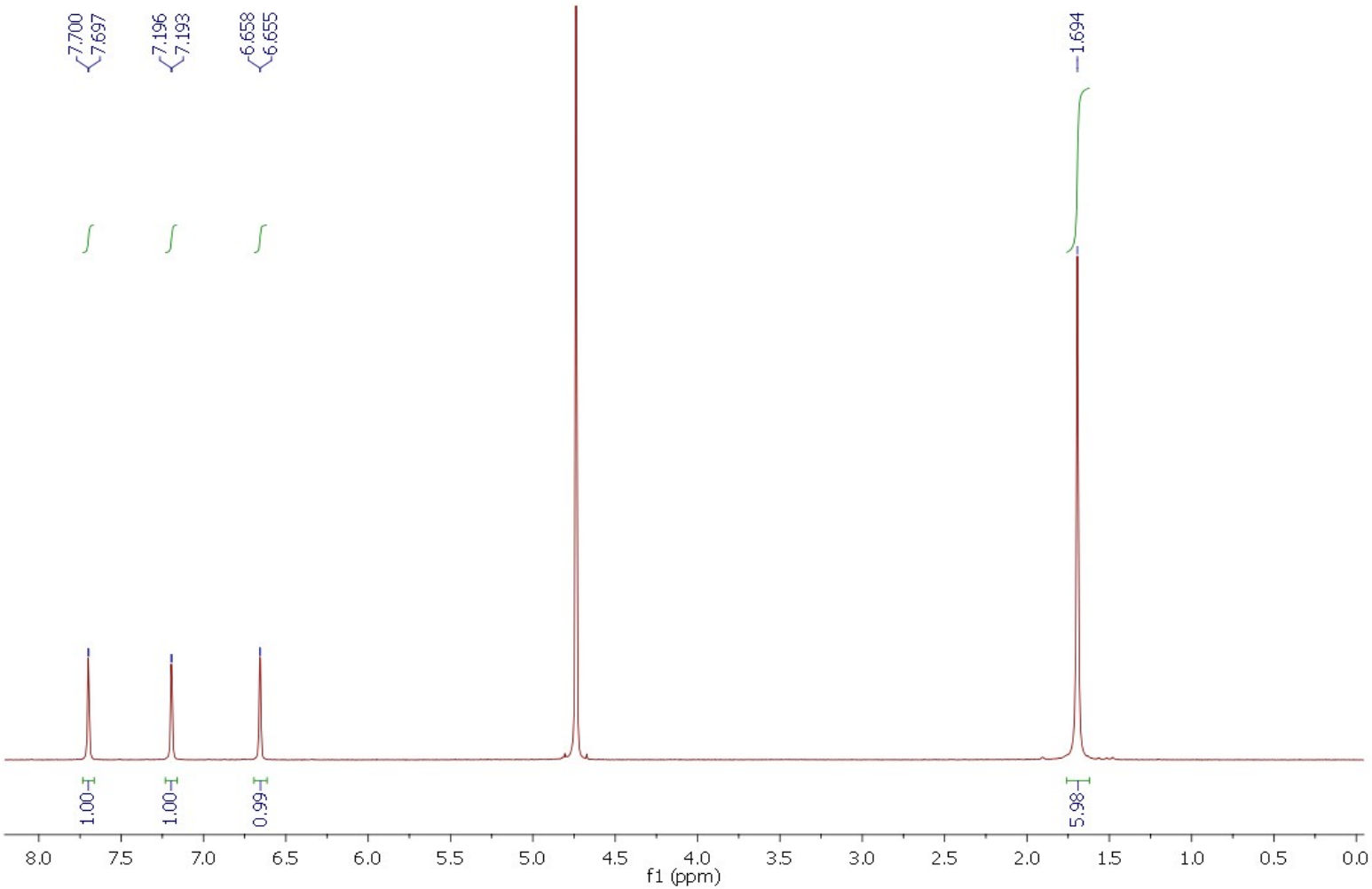

Figure S1. ^{1}H NMR spectrum of the compound **1**.

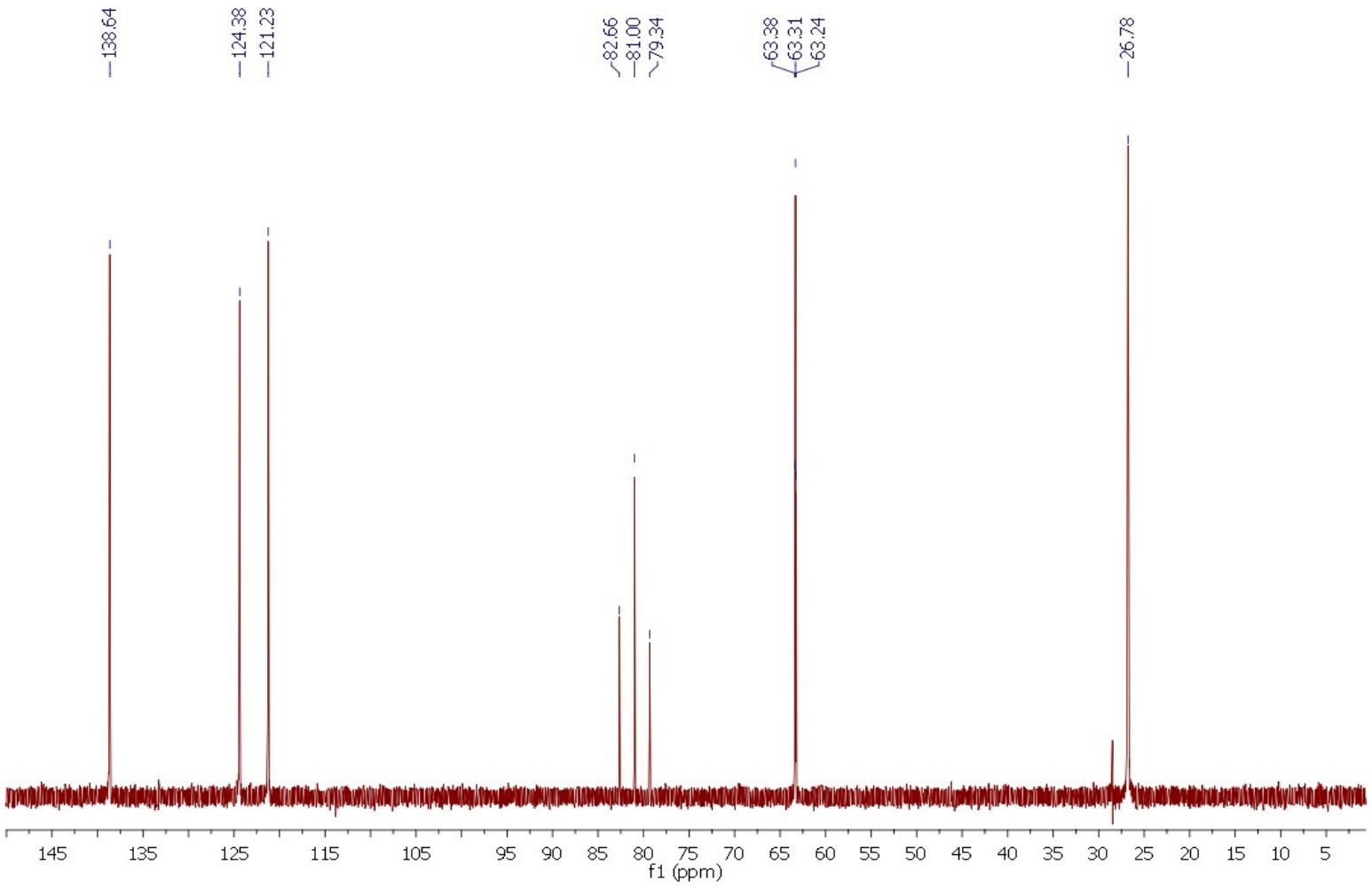

Figure S2. ^{13}C NMR spectrum of the compound **1**.

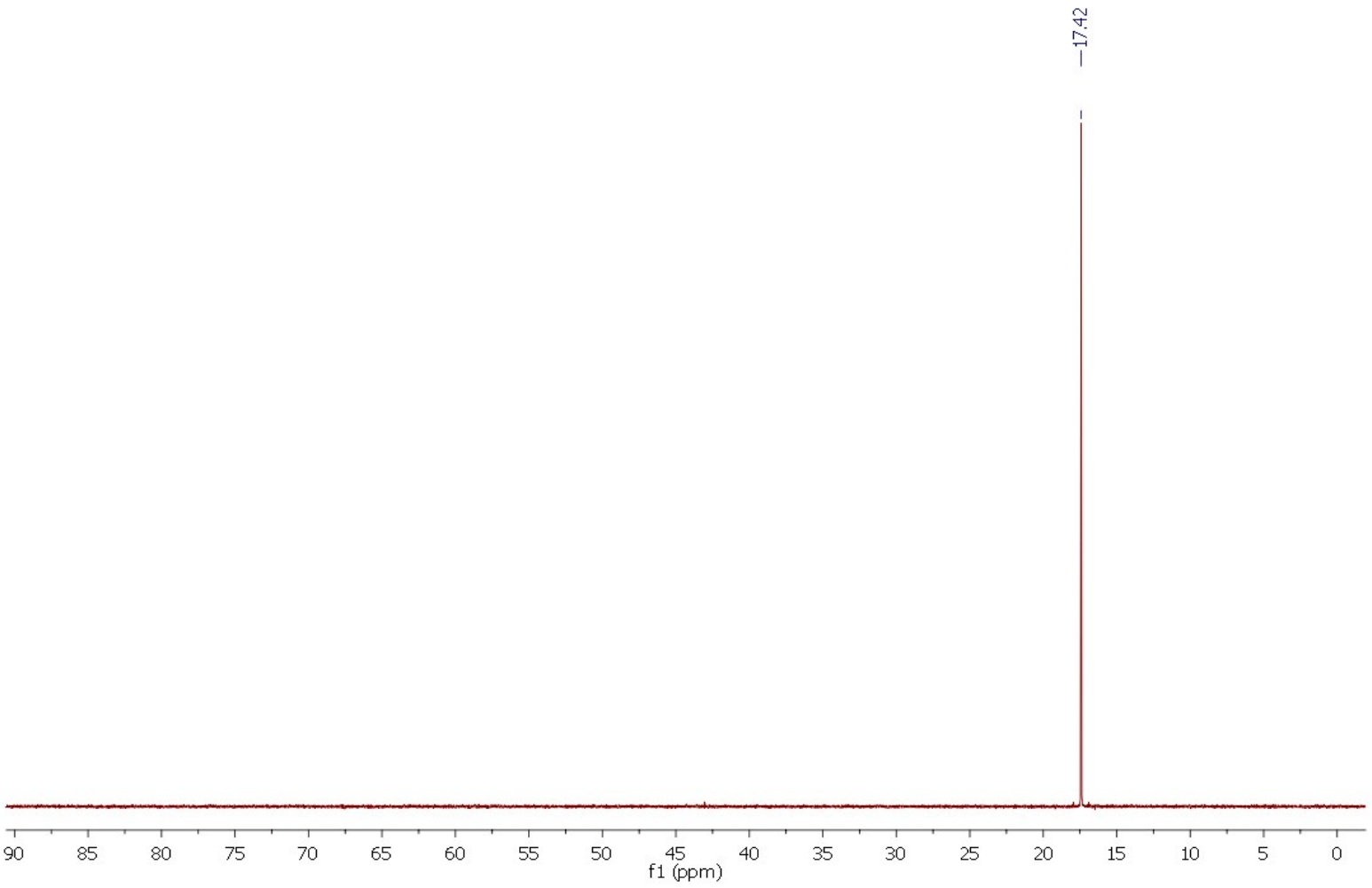

Figure S3. ^{31}P NMR spectrum of the compound **1**.

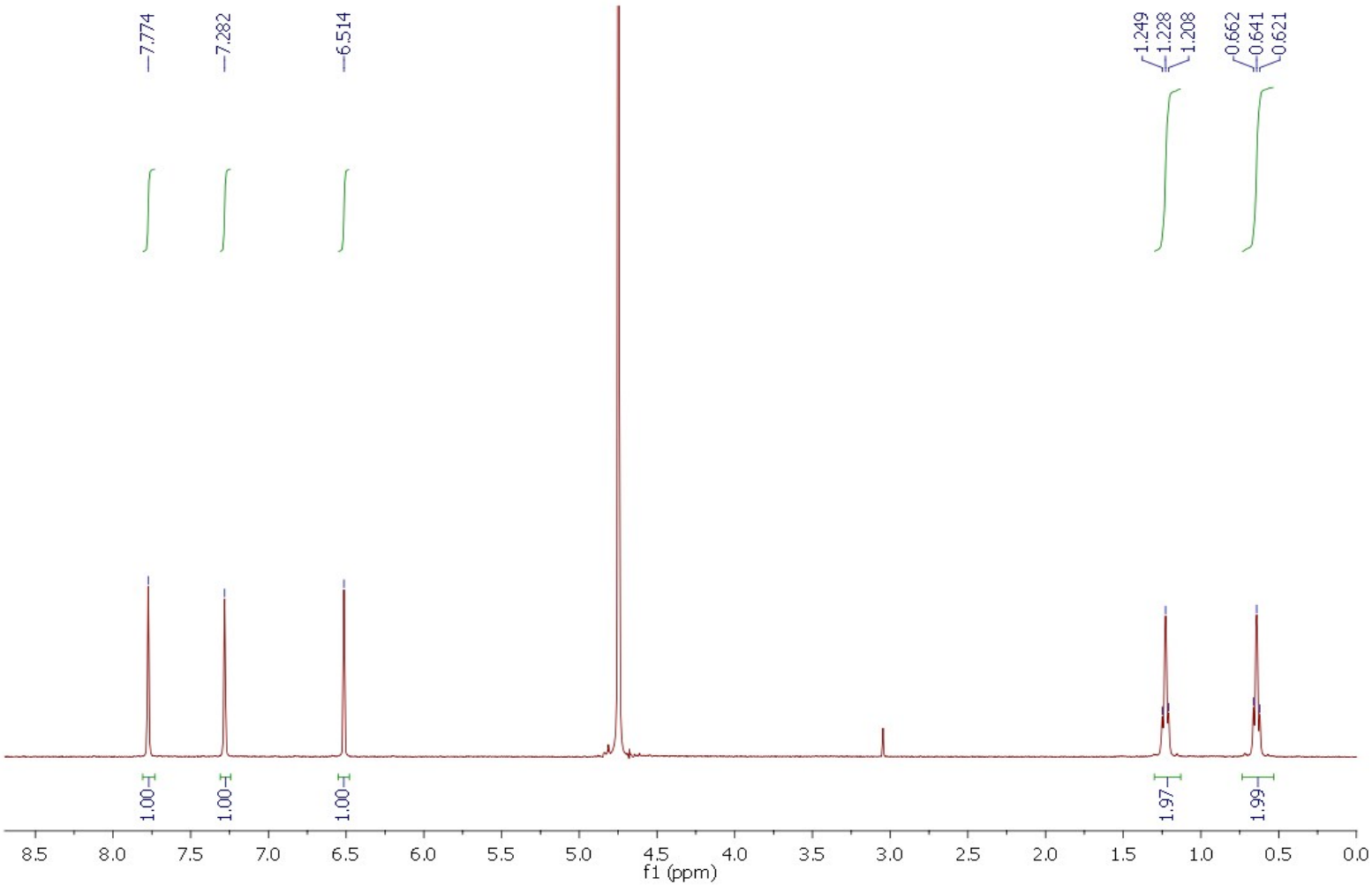

Figure S4. ^{1}H NMR spectrum of the compound **2**.

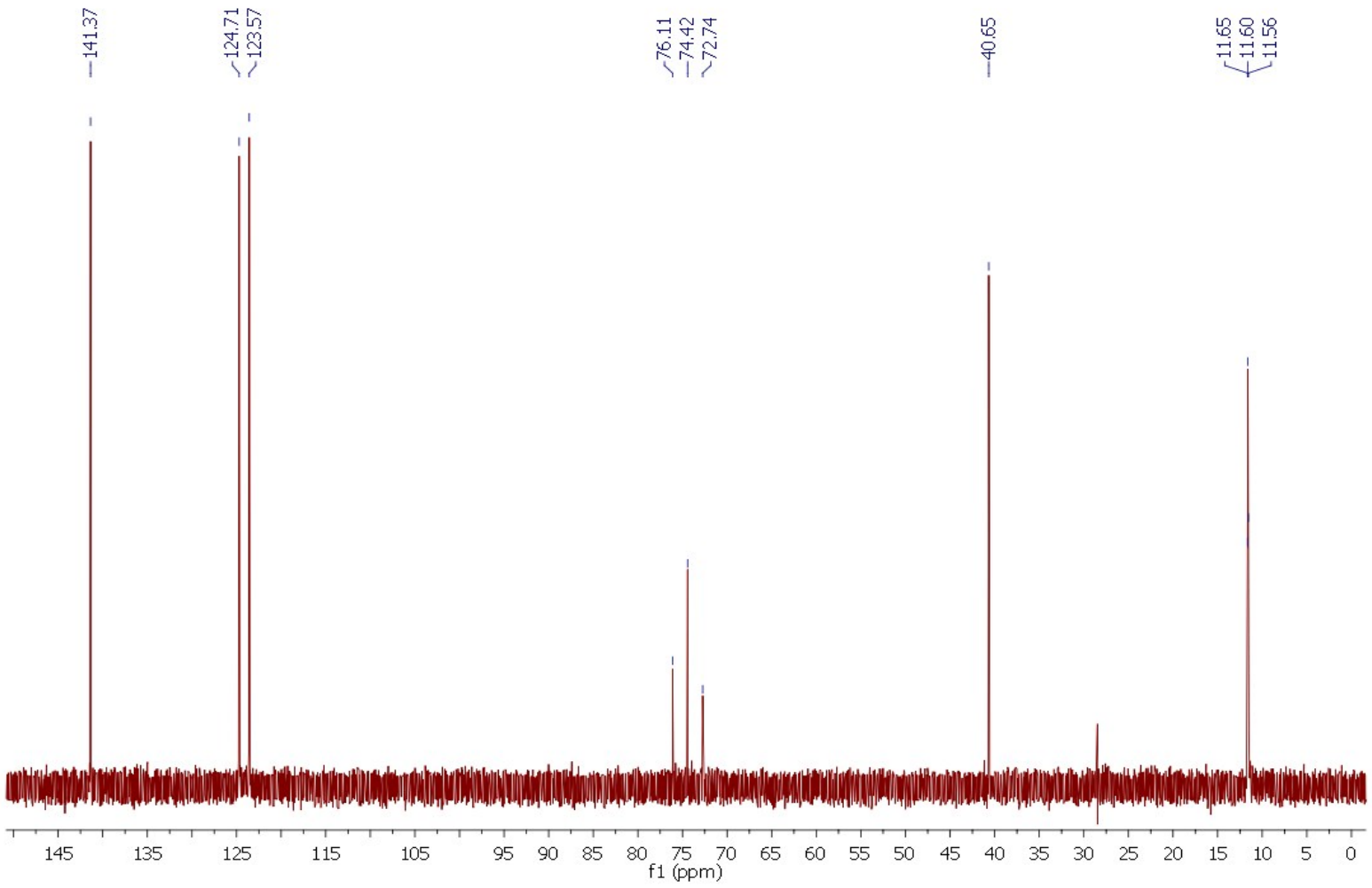

Figure S5. ^{13}C NMR spectrum of the compound **2**.

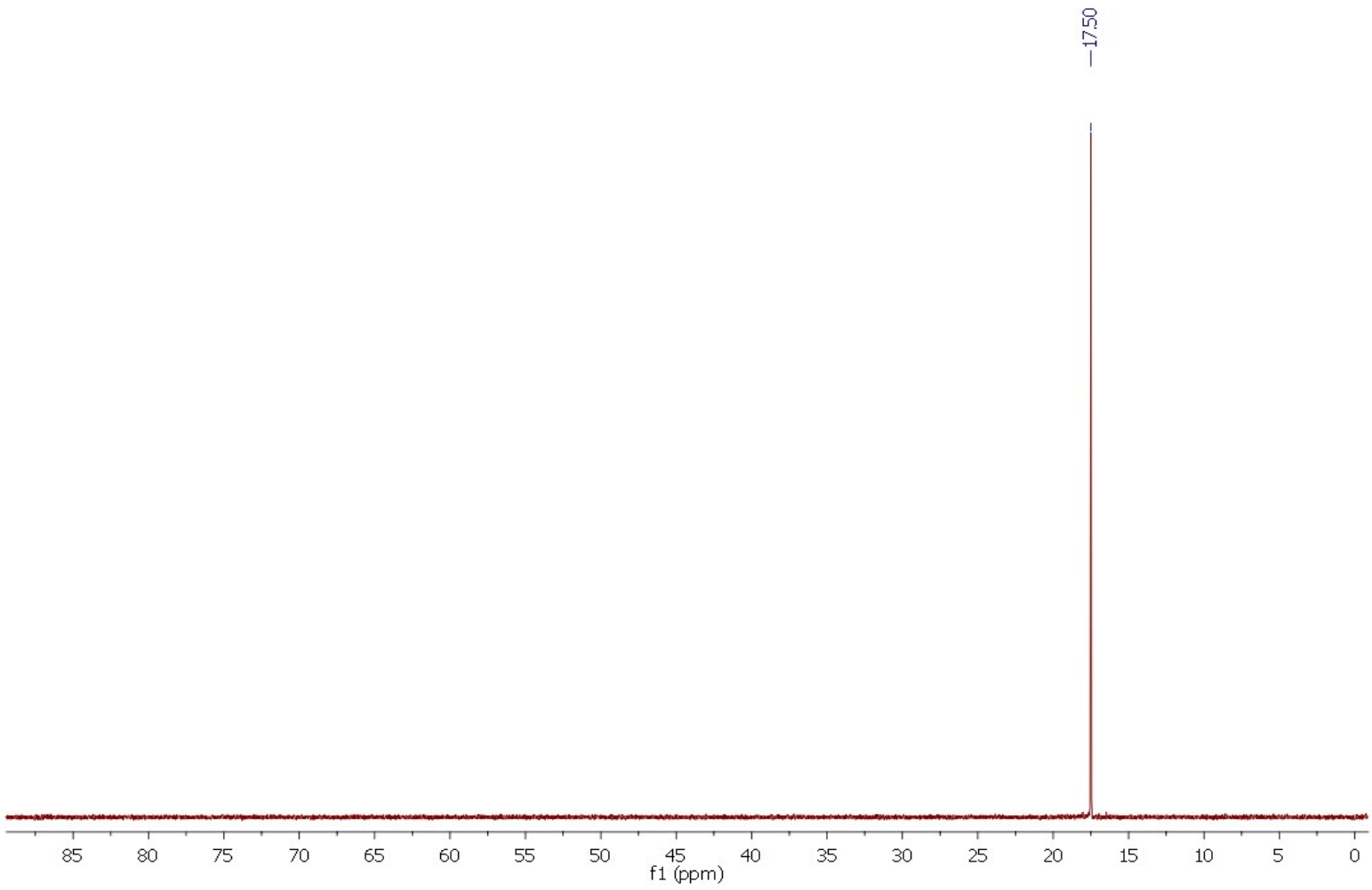

Figure S6. ^{31}P NMR spectrum of the compound **2**.

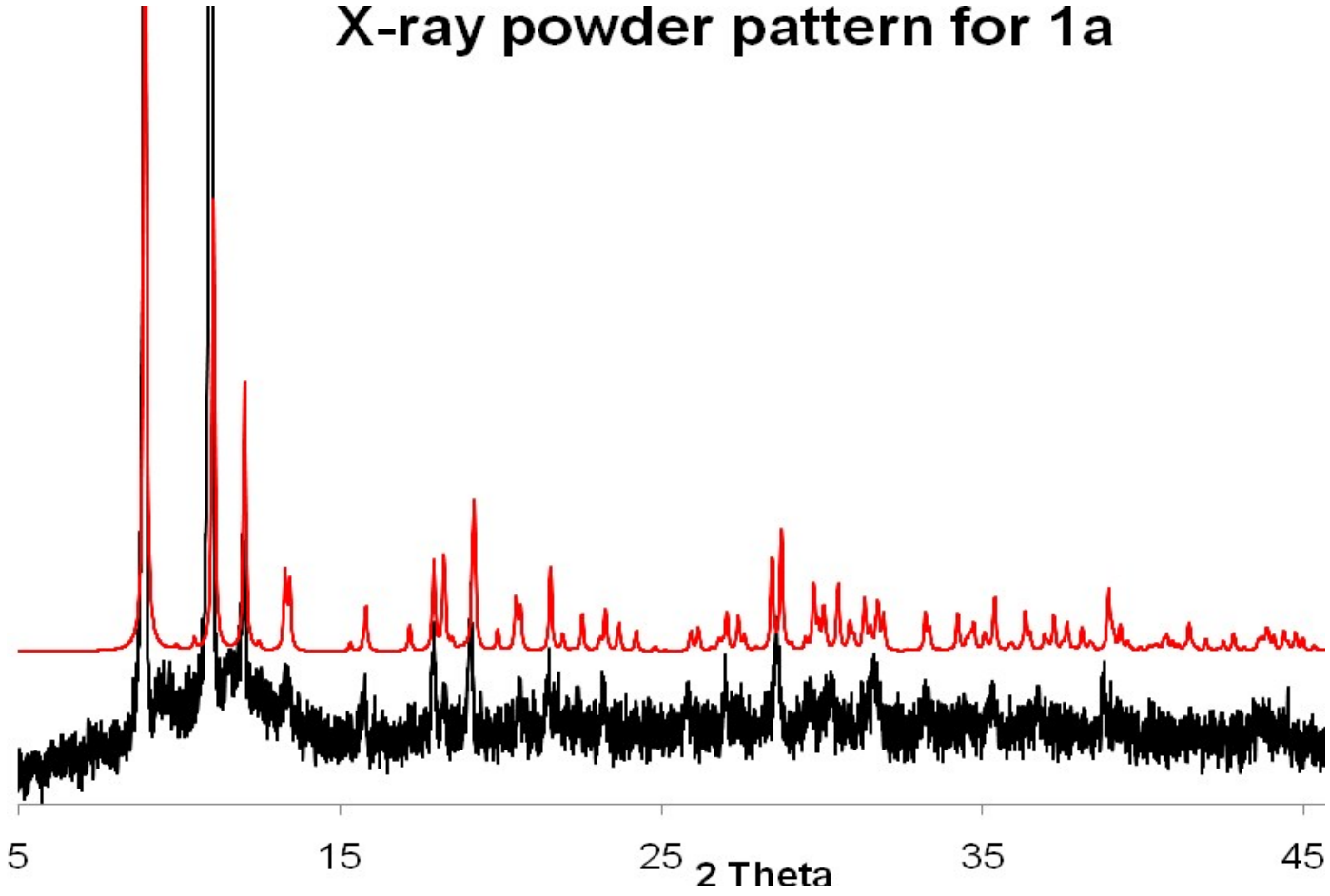

Figure S7. Experimental X-ray powder pattern (black, T = 298 K, Cu-Kα1) and simulated powder pattern (red, T = 80 K, Mo-Kα) based on the results from single-crystal X-ray diffraction for the coordination polymer **1a**.

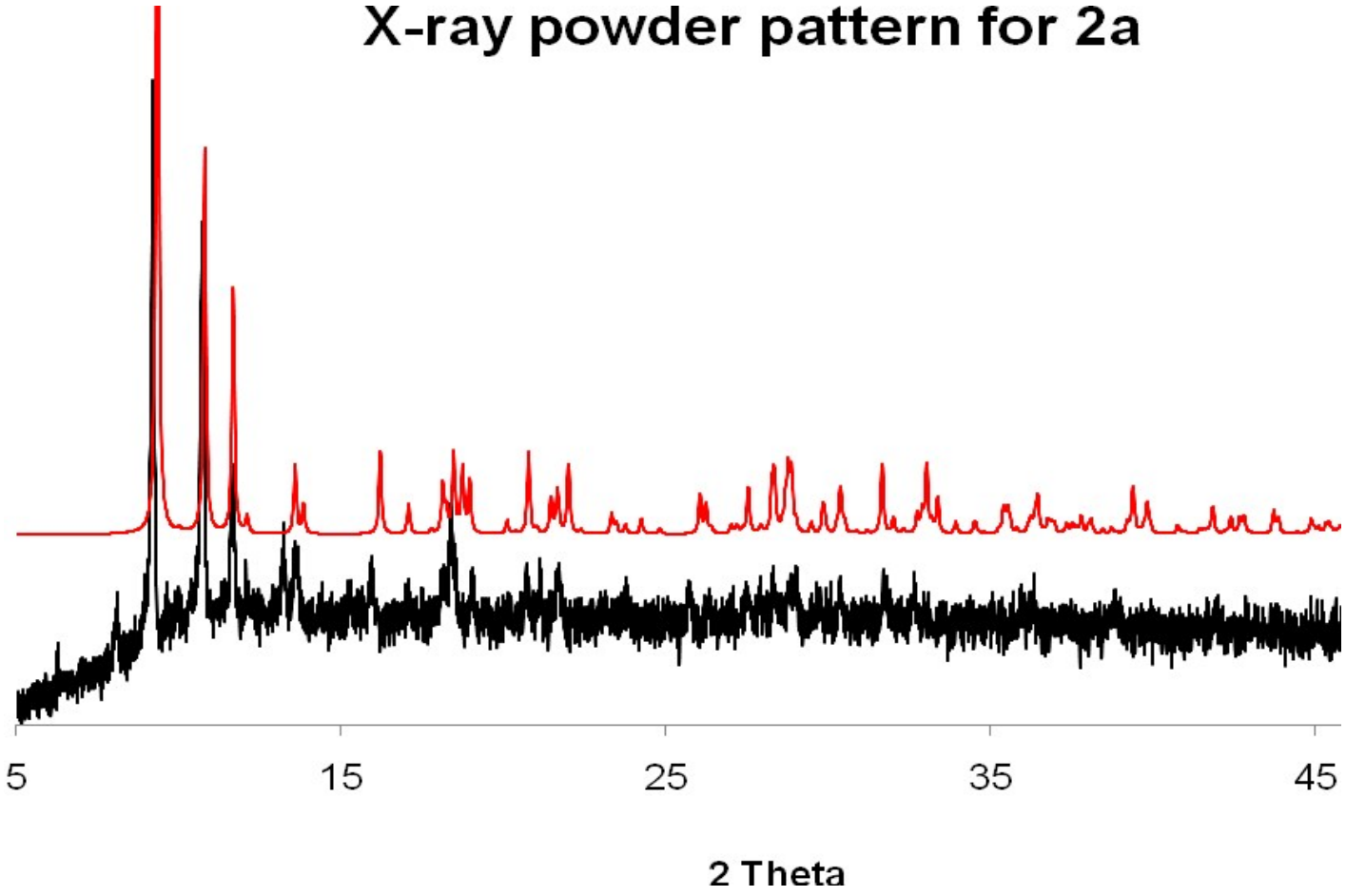

Figure S8. Experimental X-ray powder pattern (black, T = 298 K, Cu-Kα1) and simulated powder pattern (red, T = 130 K, Mo-Kα) based on the results from single-crystal X-ray diffraction for the coordination polymer **2a**.

Table S1. Selected interatomic distances (Å), bond angles (°) and torsion angles (°) for the compounds **1**, **2**, **1a** and **2a**.

	1	**2**	**1a**	**2a**
Bond lenghts				
P1–O1	1.4819(8)	1.5079(11)	1.500(2)	1.499(3)
P1–O2	1.5208(9)	1.5342(11)	1.532(3)	1.528(3)
P1–O3	1.5832(10)	1.5367(11)	1.550(3)	1.546(3)
P2–O4	1.5057(9)	1.5039(10)	1.520(2)	1.511(3)
P2–O5	1.5293(9)	1.5280(11)	1.522(3)	1.515(2)
P2–O6	1.5570(9)	1.5552(11)	1.537(3)	1.546(2)
Bond angles				
N1–C2 –C1	108.15(7)	115.63(9)	110.0(2)	113.8(3)
O1–P1–O2	115.12(5)	113.85(6)	112.34(15)	112.69(14)
O1–P1–O3	107.44(5)	114.26(6)	112.57(14)	111.96(14)
O2–P1–O3	110.94(5)	107.96(6)	110.72(14)	111.72(14)
O4–P2–O5	114.18(5)	113.32(6)	111.03(14)	111.30(13)
O4–P2–O6	112.18(5)	109.79(6)	111.06(15)	111.39(14)
O5–P2–O6	108.09(5)	109.88(6)	113.29(14)	113.33(14)
Torsion angles				
O7–C1–C2–N1	-53.81(8)	-175.49(9)	-65.3(3)	-52.9(4)
P1–C1–C2–N1	67.58(8)	-60.96(11)	49.8(3)	61.4(3)
P2–C1–C2–N1	-168.80(5)	67.88(11)	176.5(2)	-170.6(2)
O7–C1–C2–C4	-173.30(7)	39.75(12)	174.7(2)	163.5(3)
P1–C1–C2 –C4	-51.91(8)	154.28(8)	-70.2(3)	-82.2(4)
P2–C1–C2–C4	71.71(8)	-76.88(11)	56.5(3)	45.7(4)
O7–C1–C2–C3	62.76(9)	-30.61(13)	51.8(3)	90.3(4)
P1–C1–C2–C3	-175.85(6)	83.92(11)	166.8(2)	-155.4(3)
P2–C1–C2–C3	-52.23(8)	-147.24(9)	-66.4(3)	-27.4(4)

Table S2. Proposed hydrogen bonds for **1** and **2**.

D—H···*A*	*D*—H	H···*A*	*D*···*A*	*D*—H···*A*
*Compound **1***				
O2–H2···O5^{i}	1.08(4)	1.37(4)	2.4361(12)	170(4)
O3–H3···O5	0.84	2.00	2.7043(13)	141
O6–H6···O4^{ii}	0.84	1.70	2.5180(14)	163
O7–H7···O3^{iii}	0.84	2.14	2.9369(14)	159
N2–H2*N*···O1^{iv}	0.88	1.77	2.6358(14)	166
C4–H4*A*···O2	0.98	2.44	3.1016(16)	124
C4–H4*B*···O4	0.98	2.42	3.1388(16)	130
C21–H21···O5^{v}	0.95	2.49	3.3378(18)	149
C41–H41···O6^{vi}	0.95	2.57	3.0805(17)	114
C51–H51···O6^{vi}	0.95	2.57	3.0801(17)	114
C51–H51···O7^{vi}	0.95	2.60	3.5037(18)	159
*Compound **2***				
O2–H2···O2^{vii}	0.84	1.69	2.485(2)	156
O3–H3···O4^{i}	0.84	1.71	2.4934(15)	154
O5–H5···O5^{iii}	0.84	1.64	2.467(2)	166
O6–H6···O1^{viii}	0.84	1.70	2.5309(16)	171
O7–H7···O1^{viii}	0.84	1.99	2.8113(16)	165
N2–H2*N*···O1*W*^{iv}	0.88	2.26	2.904(3)	130
O1*W*–H1*W*···O4	0.84	2.04	2.856(2)	164
O1*W*–H2*W*···O1^{i}	0.84	2.55	3.291(3)	148
C3–H3*B*···O2^{vii}	0.99	2.56	3.338(2)	136
C21–H21···O5^{iii}	0.95	2.28	3.176(2)	158
C41–H41···O2^{ix}	0.95	2.21	3.1413(19)	166

*Cg*I	*Cg*J	*Cg*···*Cg*	Dihedral angle
Cg	*Cg*$^{\#}$	3.5972(15)	0

Symmetry codes: (i) −*x*+1, −*y*+1, −*z*+1; (ii) −*x*, −*y*+1, −*z*+1; (iii) −*x*+1, −*y*+1, −*z*; (iv) −*x*+1, −*y*+2, −*z*; (v) *x*, *y*+1, *z*; (vi) −*x*, −*y*+1, −*z*; (vii) −*x*+2, −*y*, −*z*+1; (viii) −*x*+1, −*y*, −*z*+1; (ix) −*x*+2, −*y*+1, −*z*+1.

(#) −*x*, −*y*+2, −*z*; *Cg* are centroids of N1–C21–N2–C41–C51 rings

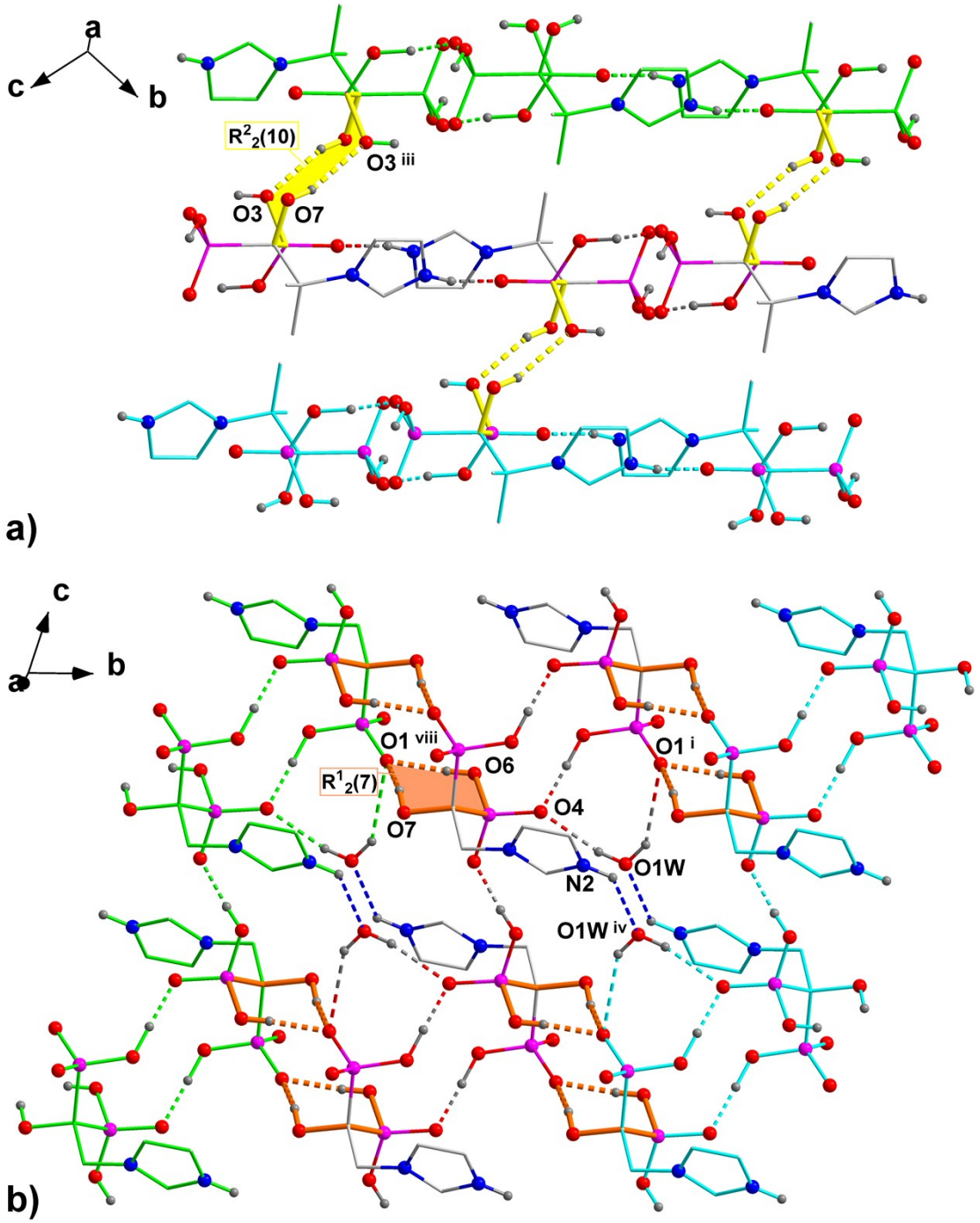

Figure S9. Arrangement of neighbouring layers (shown in bright green, grey and turquoise) into three-dimensional hydrogen-bonded network in the crystal structure of **1** (a) and **2** (b). All C-bounded H atoms, cyclopropane rings (picture b), disordered position of water molecules with lower occupancy and one from both H2 and H5 hydrogen sites with half occupancy (picture b) are omitted for clarity. Symmetry codes are given in Table 2.

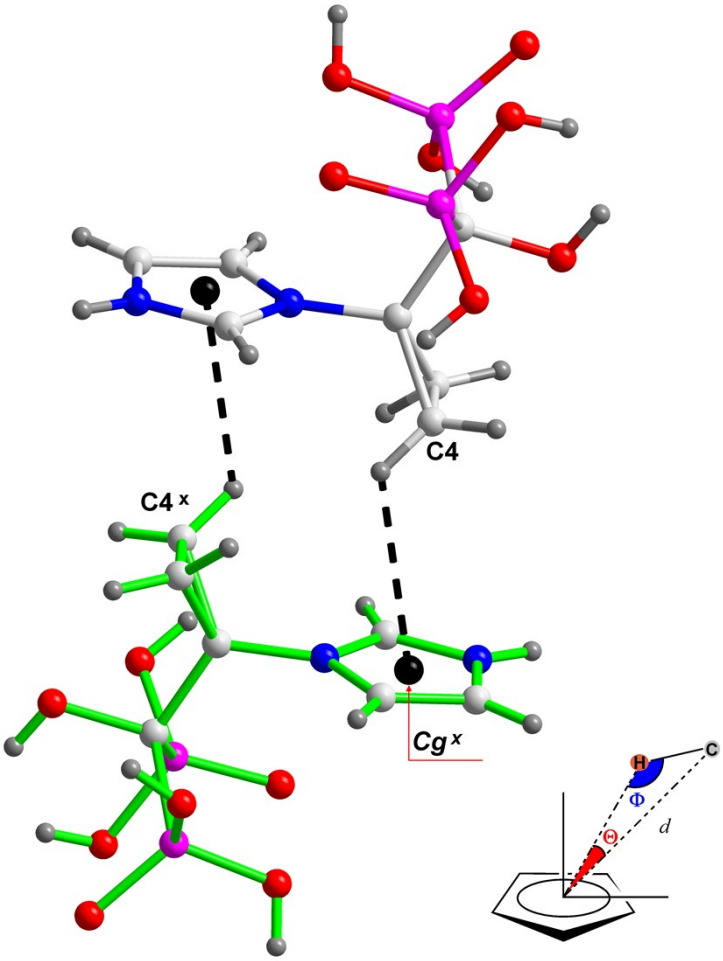

Figure S10. Illustration of C–H···π type interaction (black dashed lines) occurring between neighboring layers (constituents are shown in bright green and grey) in the crystal lattice of **2** with schematic presentation of geometric relationship in this type of contacts (shown in right bottom corner). Symmetry code: (x) −*x*+2, −*y*+1, −*z*.

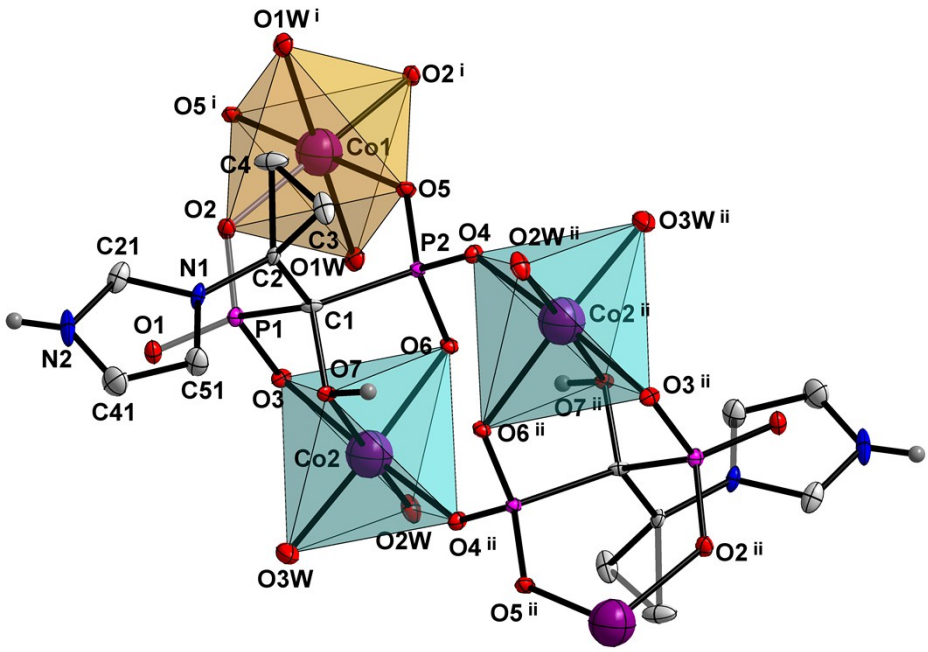

Figure S11. The coordination unit of $Co_3(HL2)_2(H_2O)_6 \cdot 6H_2O$ complex (**2a**) with the atom-numbering scheme. All H-atoms, except those attached to N2 and O7 are omitted for clarity. Displacement ellipsoids are drawn at 50 % probability level.

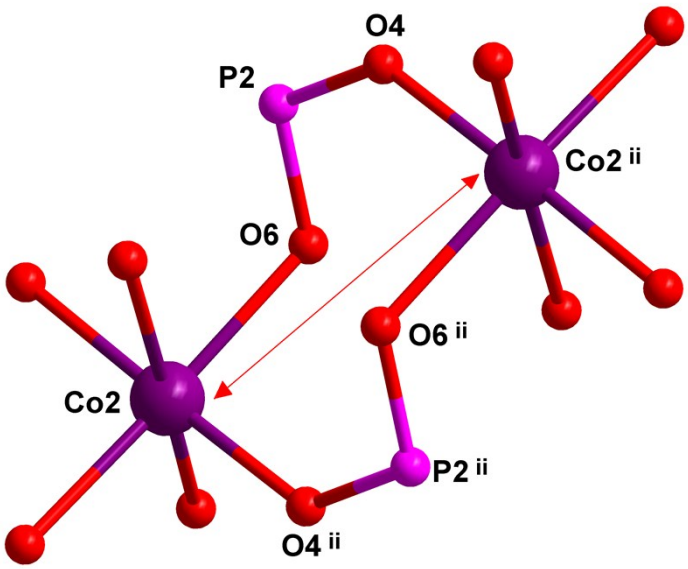

Figure S12. Formation of 8-membered ring in complexes **1a** and **2a**. Red arrow shows the Co2···Co2 distance, which is 4.7192(13) Å in case of **1a** and 4.7705(13) Å in **2a**. Symmetry code: (ii) $-x+1, -y+1, -z+1$.

Table S3. Selected interatomic distances (Å), bond angles (°) and torsion angles (°) for the compounds **1a** and **2a**.

	1a	**2a**		**1a**	**2a**
Bond lengths					
Co1–O2, O2^{i}	2.097(2)	2.061(2)	Co2–O3	2.041(3)	2.061(3)
Co1–O5, O5^{i}	2.055(3)	2.047(3)	Co2–O4^{ii}	2.005(3)	2.014(3)
Co1–O1W, O1W^{i}	2.203(3)	2.183(2)	Co2–O6	2.113(2)	2.130(2)
			Co2–O7	2.248(3)	2.211(3)
			Co2–O2W	2.108(3)	2.130(3)
			Co2–O3W	2.138(2)	2.059(3)
Bond angles					
O2–Co1–O1W	86.89(10)	87.35(10)	O3–Co2–O3W	94.42(10)	94.91(11)
O2–Co1–O1W^{i}	93.11(10)	92.65(10)	O4^{ii}–Co2–O6	91.45(10)	90.99(10)
O5–Co1–O2	89.15(10)	92.33(10)	O4^{ii}–Co2–O7	93.78(10)	91.03(10)
O5^{i}–Co1–O2	90.85(10)	87.67(10)	O4^{ii}–Co2–O2W	92.64(11)	89.89(10)
O5–Co1–O1W	91.92(10)	89.61(10)	O4^{ii}–Co2–O3W	85.94(10)	87.85(11)
O5–Co1–O1W^{i}	88.08(10)	90.39(10)	O6–Co2–O7	79.83(9)	80.78(9)
O3–Co2–O6	87.80(10)	85.85(10)	O2W–Co2–O6	97.21(9)	97.93(9)
O3–Co2–O7	83.37(10)	86.00(10)	O2W–Co2–O3W	90.64(10)	90.38(10)
O3–Co2–O2W	90.19(10)	93.02(10)	O3W–Co2–O7	92.62(9)	90.92(10)

Symmetry codes: (i) $-x+2, -y, -z+1$; (ii) $-x+1, -y+1, -z+1$

Table S4. Hydrogen bonds for **1a** and **2a**.

D—H···*A*	*D*—H	H···*A*	*D*···*A*	*D*—H···*A*
*Compound **1a***				
O7–H7*O*···O6^{ii}	0.84	1.97	2.740(4)	152
N2–H2*N*···O2^{iii}	0.88	1.81	2.688(4)	171
O1*W*–H1*W*···O3	0.84	1.88	2.712(4)	170
O1*W*–H2*W*···O5*W*	0.84	2.01	2.801(5)	158
O2*W*–H3*W*···O3^{iv}	0.84	1.94	2.772(4)	173
O2*W*–H4*W*···O5*W*	0.84	1.99	2.812(4)	165
O3*W*–H5*W*···O1*W*^{iv}	0.84	2.11	2.903(3)	157
O3*W*–H6*W*···O4*W*	0.84	1.95	2.738(4)	155
O4*W*–H8*W*···O1	0.84	1.80	2.643(4)	178
O5*W*–H9*W*···O4*W*^{v}	0.84	2.13	2.783(4)	134
O5*W*–H10*W*···O4*W*$'^{iv}$	0.84	1.94	2.778(4)	172
O6*W*–H12*W*···O4^{ii}	0.84	2.23	2.894(5)	136
O6*X*–H12*X*···O5^{vi}	0.84	2.19	2.804(6)	130
C3–H3*B*···O4	0.98	2.31	2.994(5)	126
C4–H4*A*···O2	0.98	2.45	3.208(4)	134
C21–H21···O1^{iii}	0.95	2.45	3.101(5)	126
*Compound **2a***				
O7–H7*O*···O6^{ii}	0.84	1.95	2.771(4)	167
N2–H2*N*···O2^{iii}	0.86	1.94	2.781(4)	164
O1*W*–H1*W*···O3	0.84	1.97	2.794(3)	167
O1*W*–H2*W*···O5*W*	0.84	2.22	2.960(4)	147
O2*W*–H3*W*···O3^{iv}	0.84	1.94	2.778(3)	172
O2*W*–H4*W*···O5*W*	0.84	2.33	3.100(4)	153
O3*W*–H5*W*···O6*W*	0.84	1.98	2.734(4)	149
O3*W*–H6*W*···O4*W*	0.84	1.89	2.712(4)	165
O4*W*–H7*W*···O5*W*^{vii}	0.84	1.93	2.764(5)	176
O4*W*–H8*W*···O1	0.84	1.77	2.610(4)	177
O5*W*–H9*W*···O6	0.84	1.97	2.801(4)	171
O5*W*–H10*W*···O4*W*$'^{iv}$	0.84	2.14	2.852(5)	143
O6*W*–H11*W*···O5^{vi}	0.84	1.92	2.744(3)	167
O6*W*–H12*W*···O2*W*	0.84	2.18	2.903(4)	145
C3–H3*B*···O4	0.99	2.18	2.954(5)	134
C4–H4*A*···O1*W*^{i}	0.99	2.46	3.320(5)	145
C21–H21···O1^{iii}	0.95	2.29	3.061(5)	137

Symmetry codes: (i) $-x+2, -y, -z+1$; (ii) $-x+1, -y+1, -z+1$; (iii) $-x+2, -y, -z$; (iv) $-x+1, -y, -z+1$; (v) $x, y, z+1$; (vi) $x-1, y, z$; (vii) $x, y, z-1$

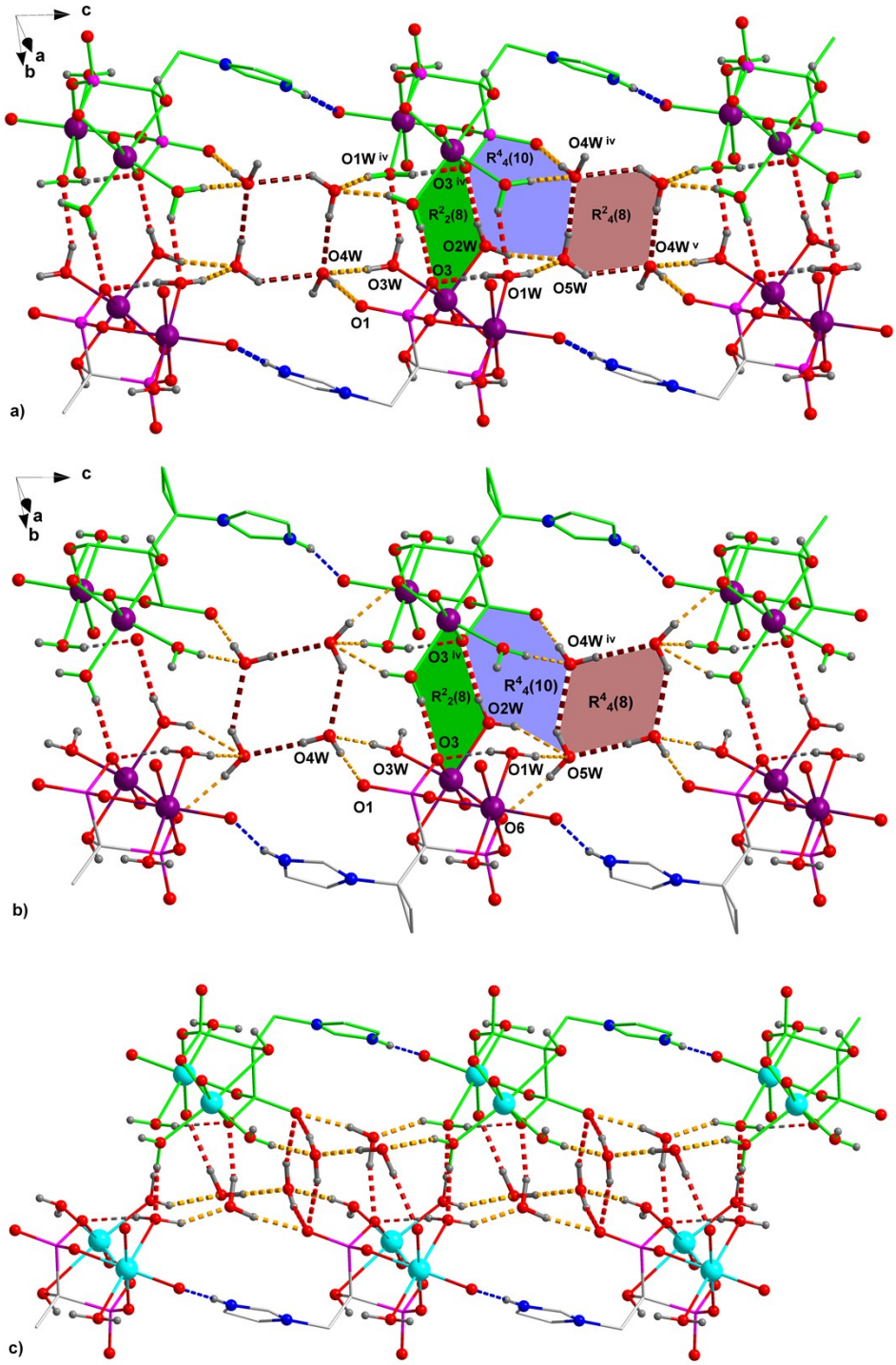

Figure S13. Packing modes of the layers in **1a** (a), **2a** (b) and $Cu_3(HZol)_2(H_2O)_6 \cdot 6H_2O$ complex (c) [25]. All H atoms not involved in the creation of hydrogen bonds and O6W lattice water molecules in the pictures a and b are omitted for clarity. Two adjacent layers are shown in bright green and light grey.

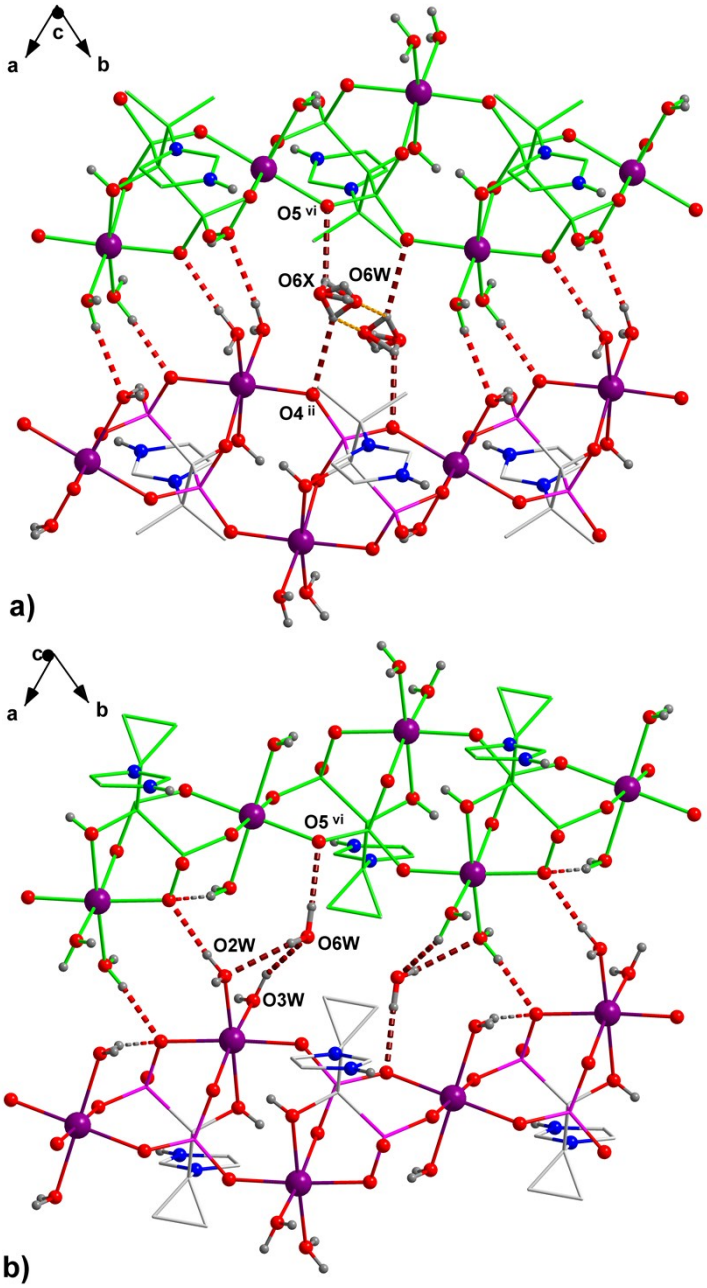

Figure S14. Role of O6W lattice water molecule in stabilization of the 3D network in complexes **1a** (a) and **2a** (b). All H atoms not involved in the creation of hydrogen bonds and O4W, O5W lattice water molecules are omitted for clarity. Two adjacent layers are shown in bright green and light grey.

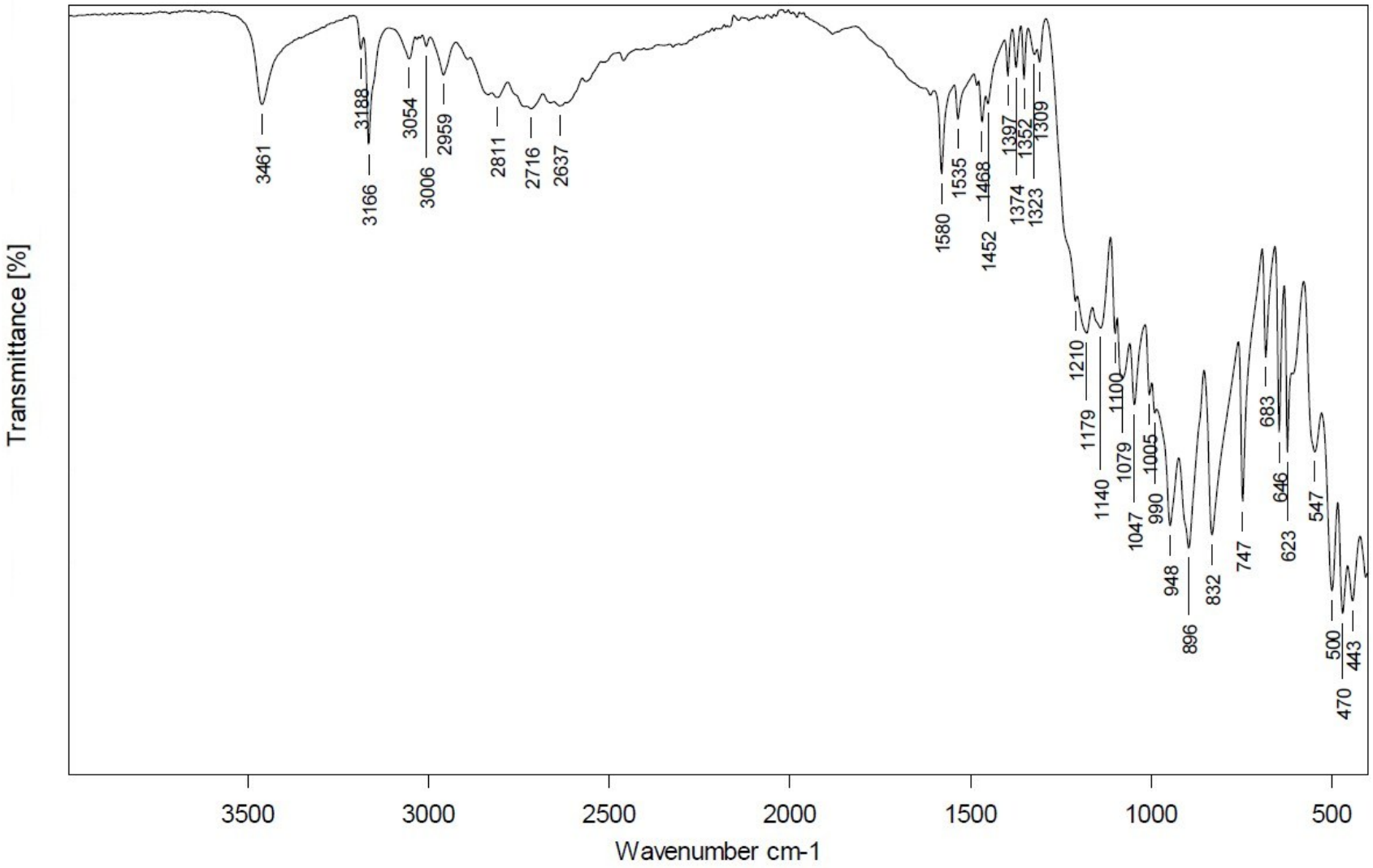

Figure S15. IR spectrum of **1**.

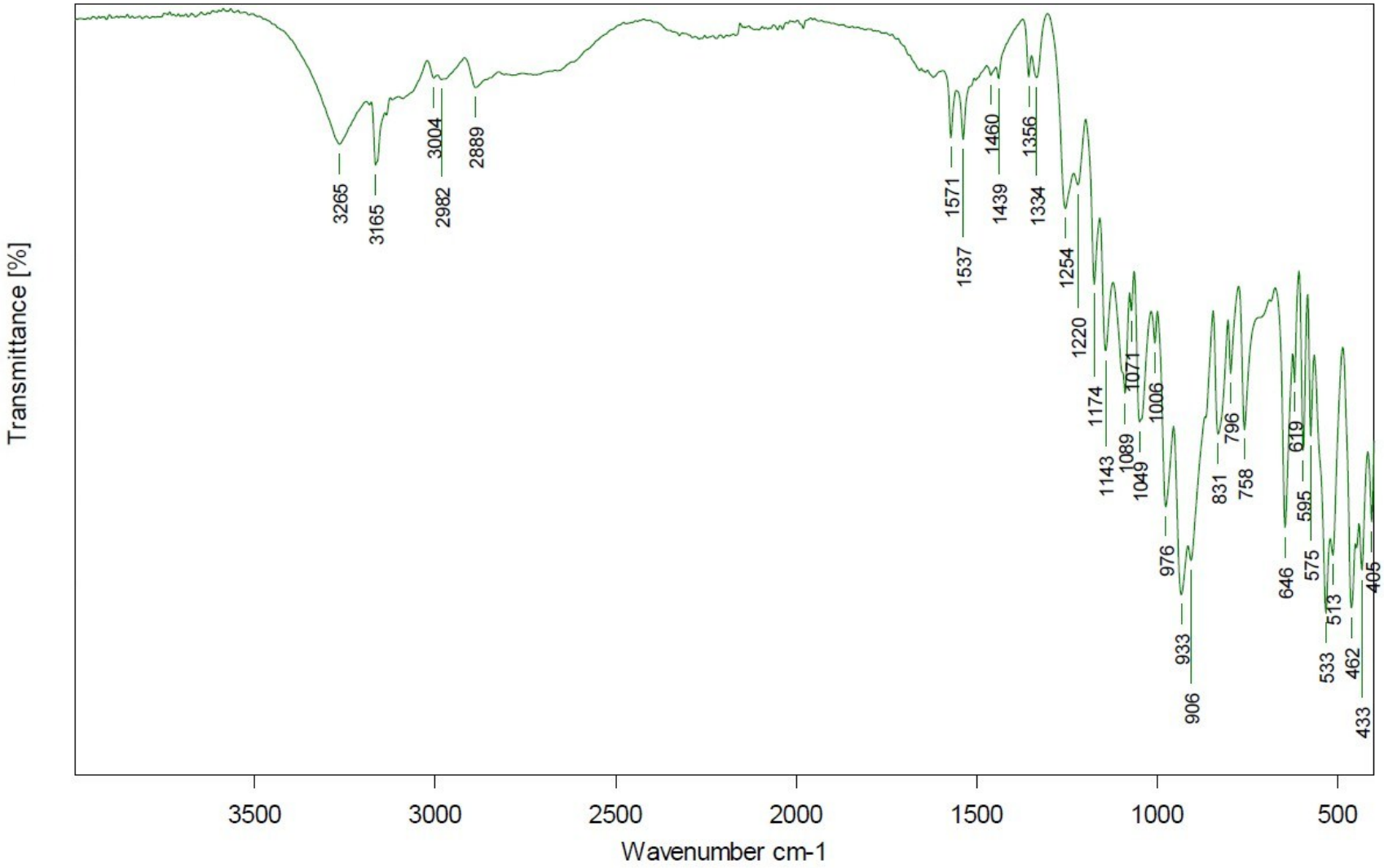

Figure S16. IR spectrum of **2**.

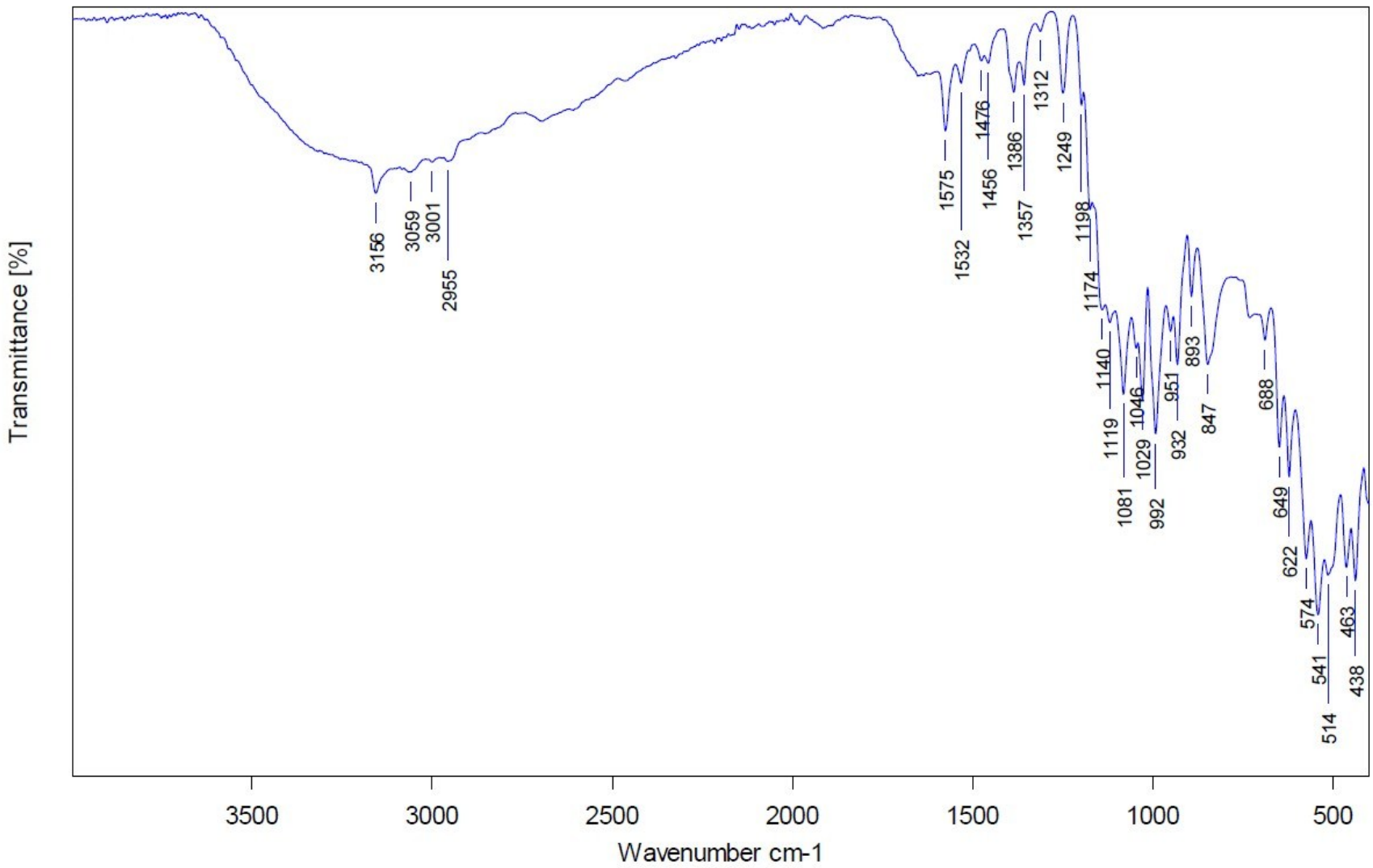

Figure S17. IR spectrum of **1a**.

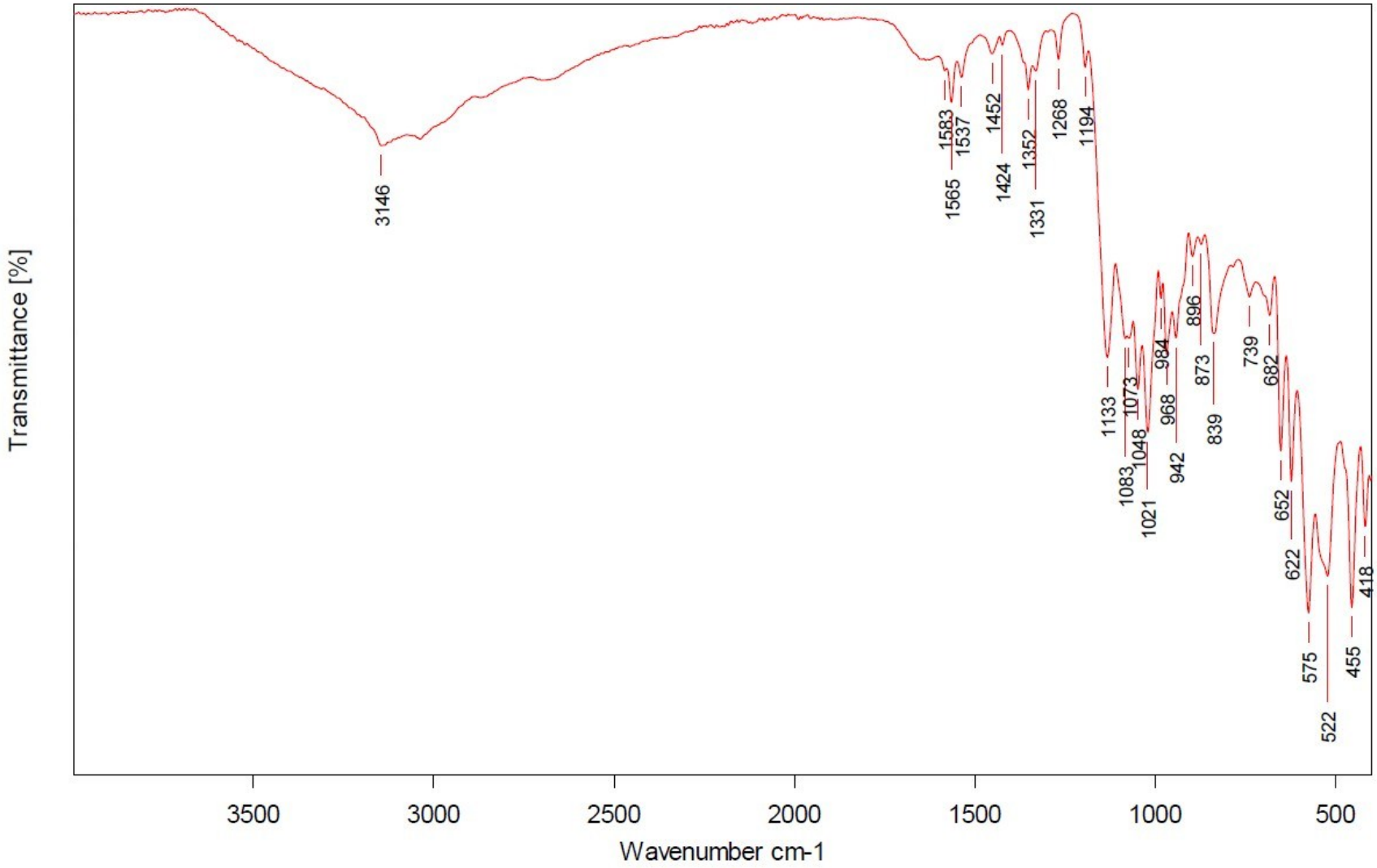

Figure S18. IR spectrum of **2a**.

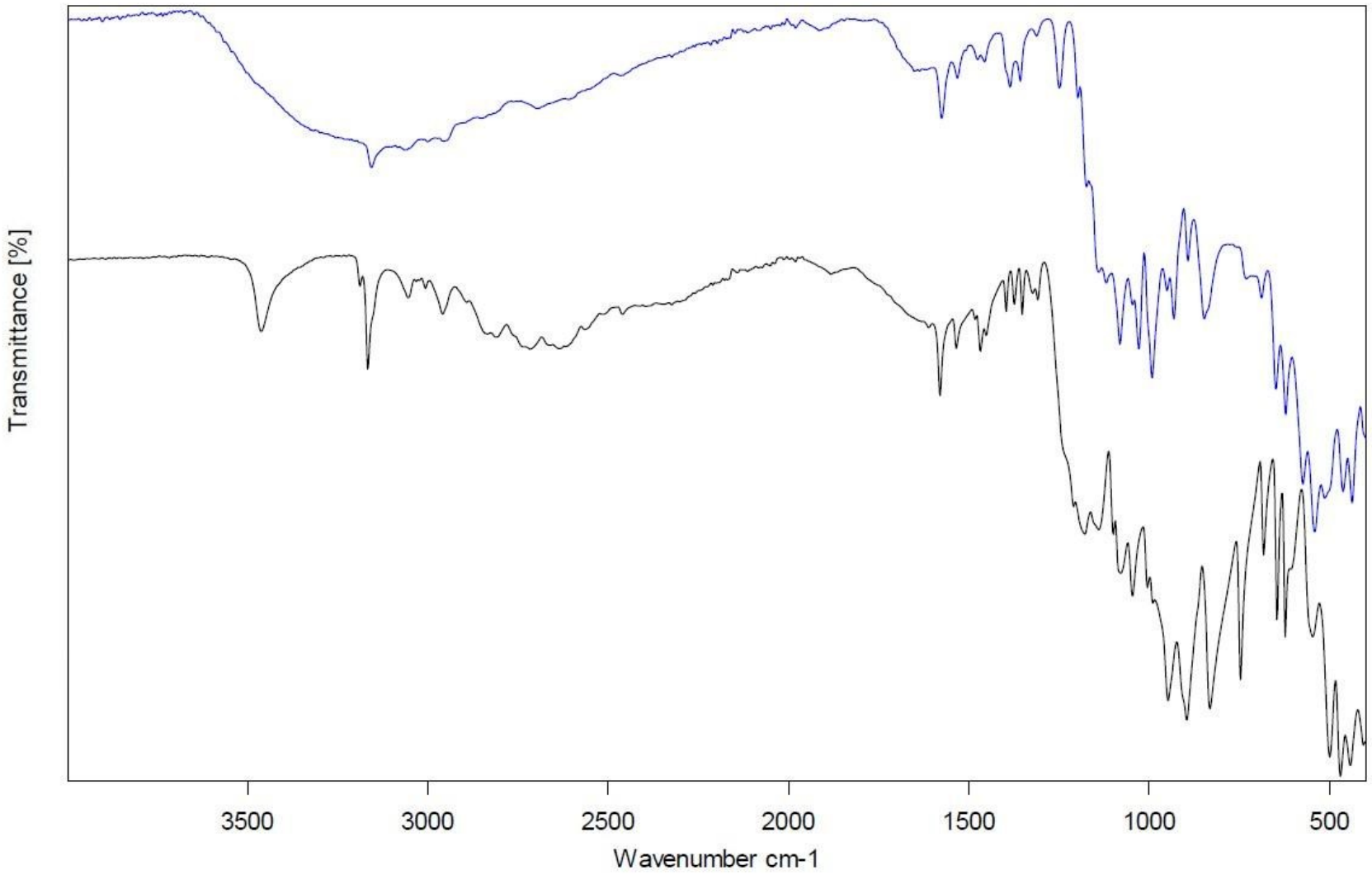

Figure S19. A comparison of IR spectra of ligand **1** (black line) and its coordination polymer **1a** (blue line).

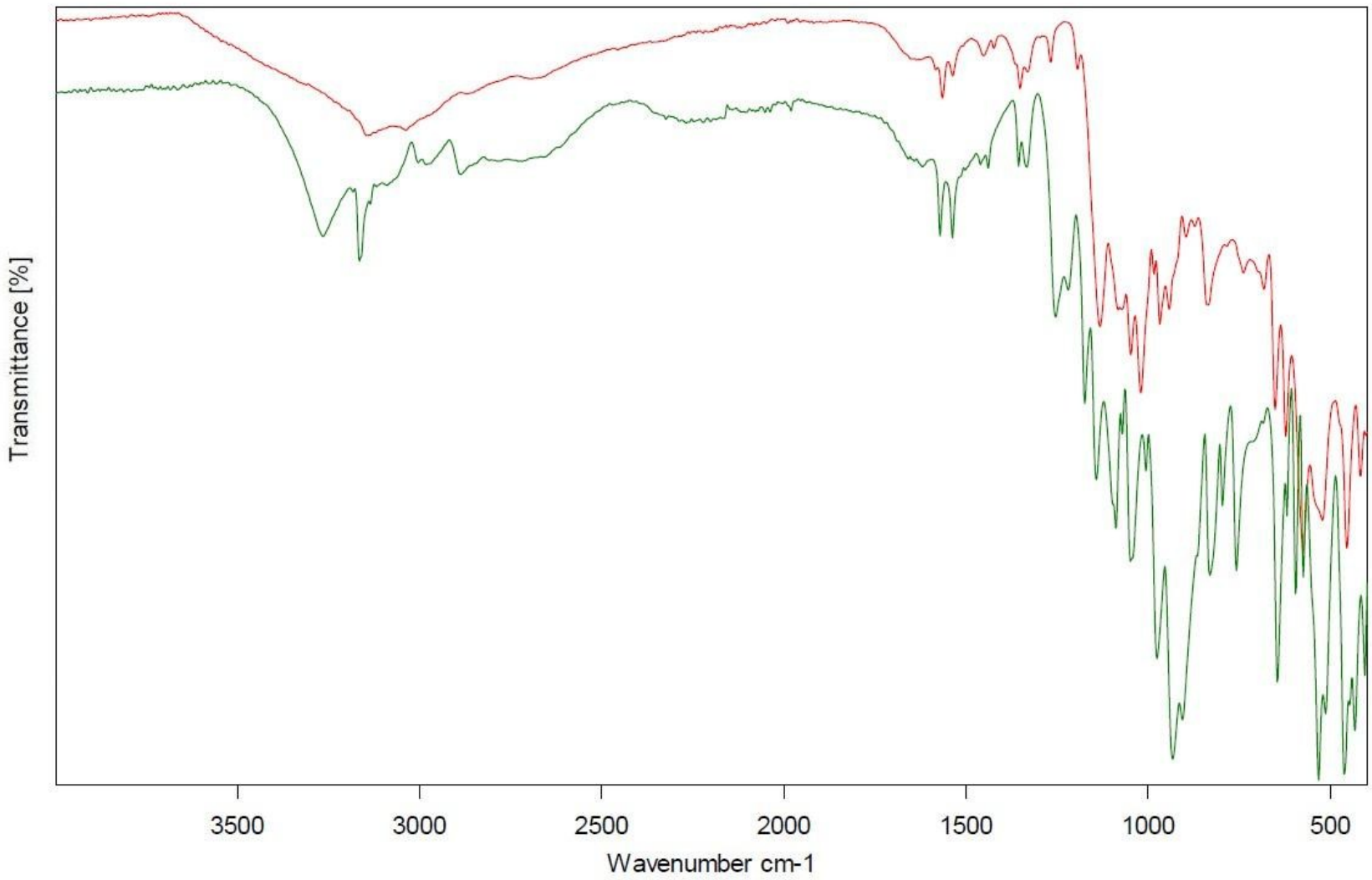

Figure S20. A comparison of IR spectra of ligand **2** (green line) and its coordination polymer **2a** (red line).

Table S5. Tentative assignments of the observed IR bands [cm^{-1}] for ligands **1** and **2** and related coordination compounds **1a** and **2a**.

compound		Band assignment[b]	compound	
1	**2**		**1a**	**2a**
3461	3265	ν(O–H)	3500-3200 br[a] (mostly O–H···O)	3500-3200 br (mostly O–H···O)
3166	3165	ν(N–H)/im	3156 br	3146 br
3054 3006		ν_{as}(C–H)/im	3059	
2959		ν_s(C–H)/CH_3	3001	
	3004	ν_s(C–H)/im		
	2982	ν_{as}(C–H)/im	2955	
	2889	ν_s(C–H)/CH_2		
2716 br 2637 br	2728 br 2660 br	ν(P–OH)		
	1655 br	δ(H_2O)	1663 br	1650 br
1580 1535 1468 1452	1571 1537 1460 1439	ν(C=C)/im; ν(N=C)/im, ν(N–C)/im	1575 1532 1476 1456	1565 1537 1452 1424
1397 1374		δ(CCH_3); δ(CH_3)	1386	
1352	1356	ν(N–C)/im	1357	1352
1323 1309		δ(PO–H); δ(CCH_3); δ(CH_3)	1312	
	1334	δ(PO–H); δ(CH_2)		1331
1240 sh 1210	1254 1220	ν(C–C)/im	1249	1268
1179	1174	ν(P=O)	1198	1194
1079	1089	δ(C–H)	1081	1083
1047	1049	ν(C–OH)	1046	1048
		ν(P–O)	1029	1021
1005	1006	ν(N–C)/im	1004	1004
948 br	976 933	ν(P–O)	951 932	968 942
896	906	ν(P–O)	893	895 871
832	831	ν(P–O)	847	839
	796	ρ_r(CH_2)		784 br
747	758	γ(POH)		
646	646	ν(C–P)	649	652
623	619	π(C–H)/im	622	622
601 sh	595 575	τ_1/im	574	575
547	533 514	δ(O–P–O); δ(C–P)	541	522
500	513		514	522
470	462		463	455
443	433		438	418

[a] sh – shoulder. br - broad

[b] ν_a – antisymmetric stretching, ν_s – symmetric stretching, δ – bending in-plane, π – bending out of plane, ρ_r – rocking, γ – torsion

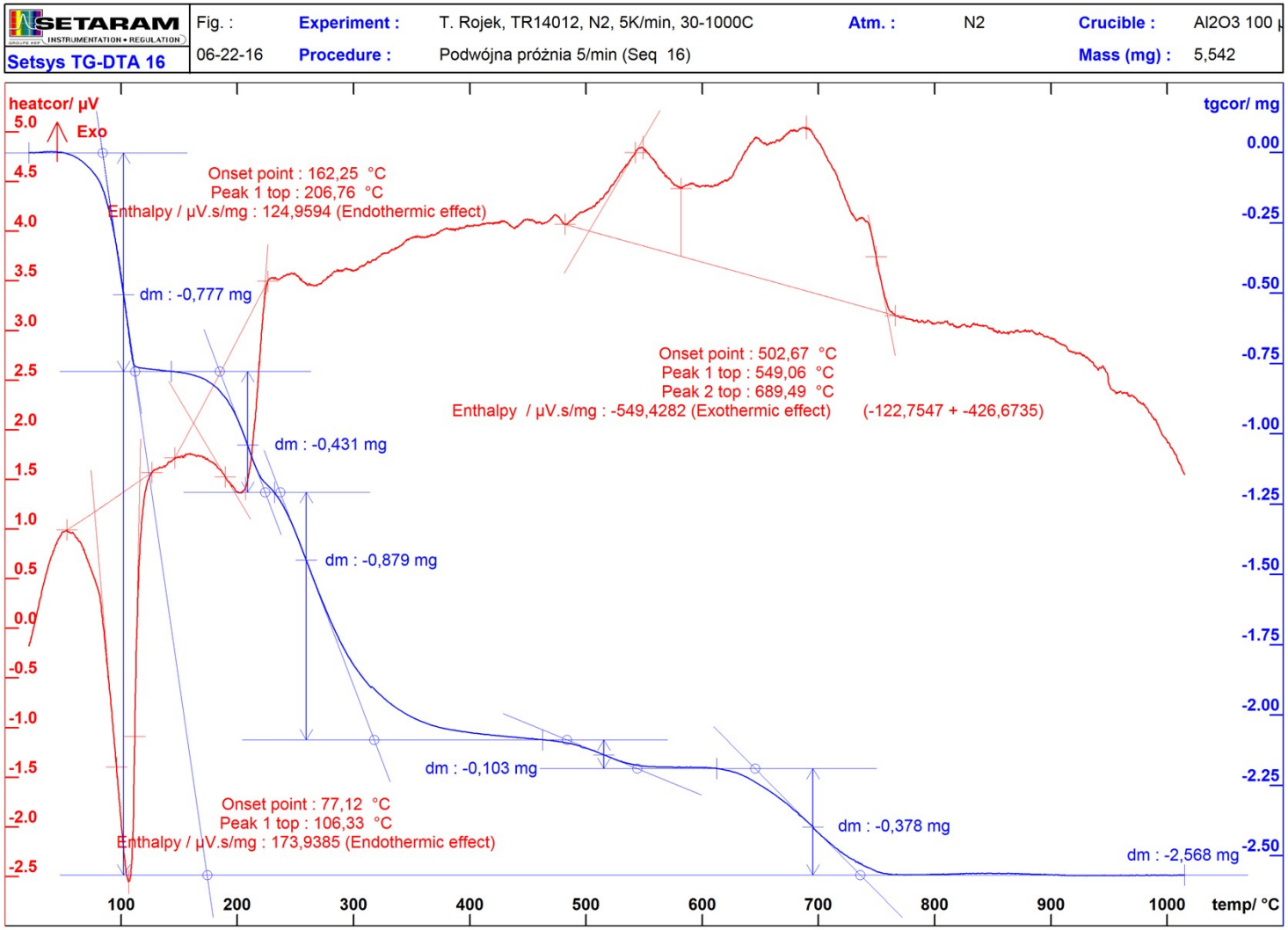

Figure S21. TG-DTA plot for the compound **1a**.

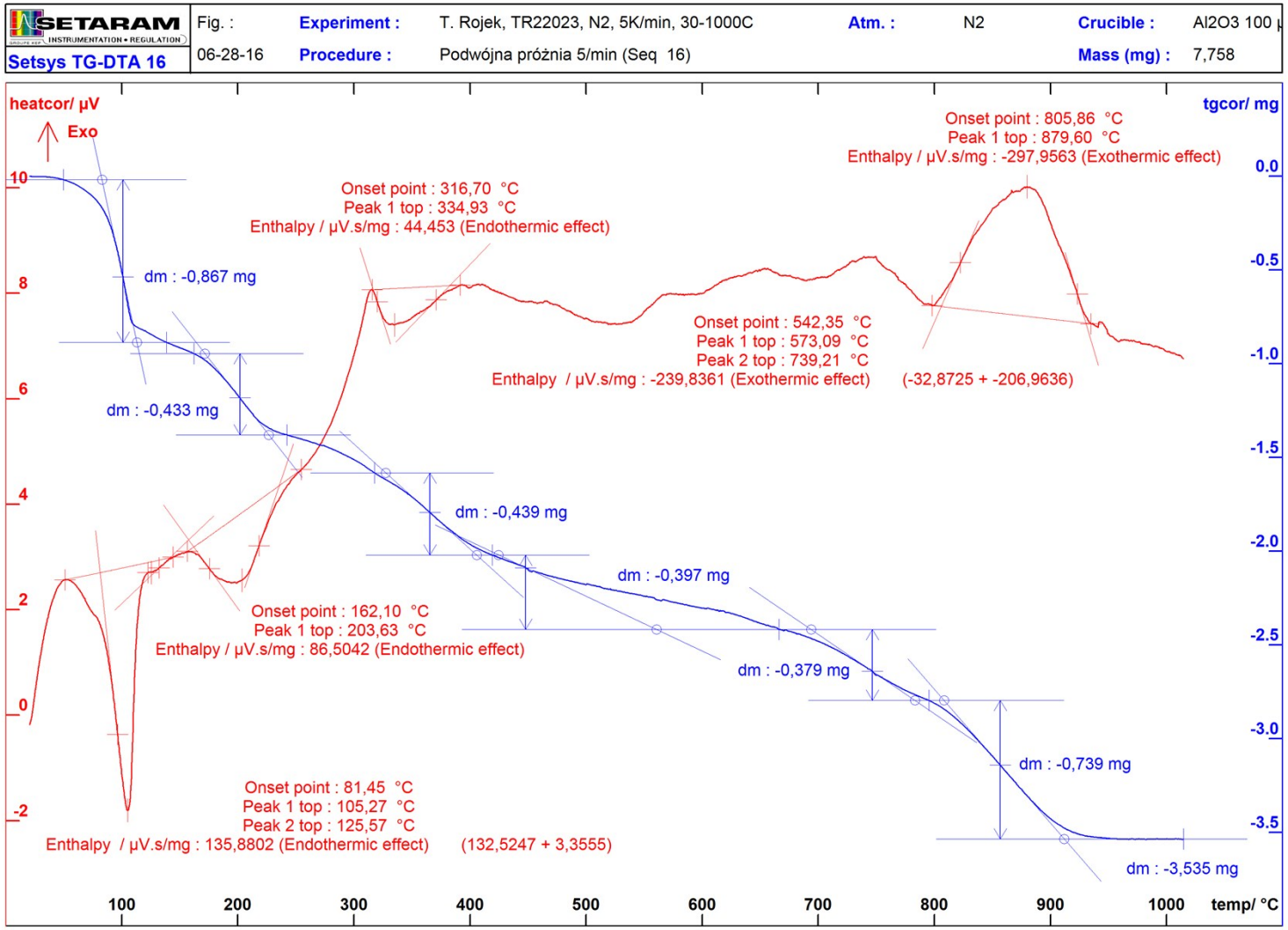

Figure S22. TG-DTA plot for the compound **2a**.

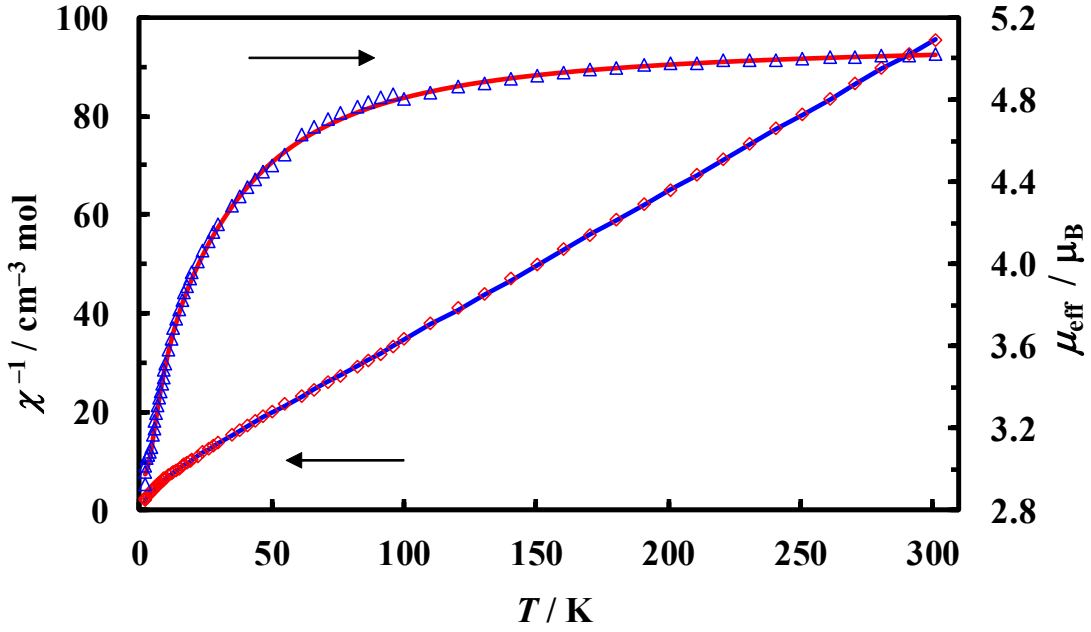

Figure S23. Temperature dependence of the effective magnetic moments of **1a** (triangles) and the reciprocal magnetic susceptibility (diamonds). Solid lines show the best fit of the data according to model **C**.

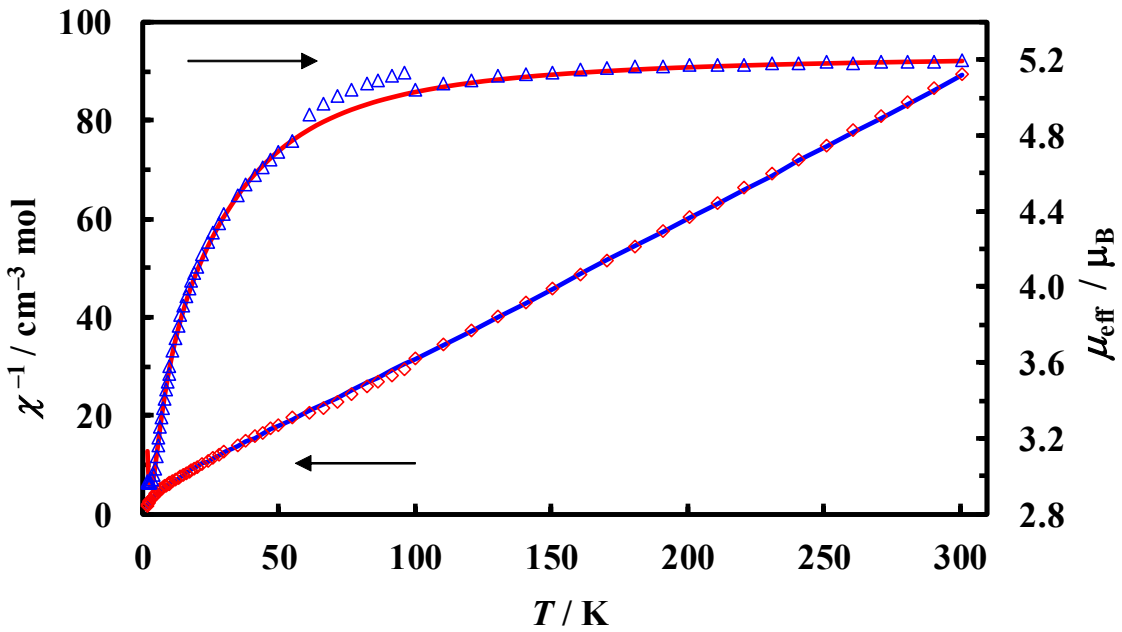

Figure S24. Temperature dependence of the effective magnetic moments of **2a** (triangles) and the reciprocal magnetic susceptibility (diamonds). Solid lines show the best fit of the data according to model **C**.

$J_1J_1J_2$ alternating chains (model B)

The magnetic pathways in **1a** and **2a** consist of the symmetric linear Co2Co1Co2 trimers, held by the phosphonate bridges O2–P1–O3 and O5–P2–O6. Two peripheral Co2 atoms are connected to adjoining trinuclear units with the double O4–P2–O6 bridges, creating finally a *zig-zag* chain. Thus, from a magnetic point of view, the two complexes consist of $J_1J_1J_2$ alternating chains.Using the Hamiltonian:

$$H = -J_1\sum(S_{3i}S3_{i+1} + S_{3i+1}S_{3i+2}) - J_2\sum S_{3i-1}S_{3i} \quad (1)$$

Abu-Youssef [1] has derived the exact expression for magnetic susceptibility of $J_1J_1J_2$ alternating chain with Heisenberg-type exchange between the classical spins:

$$\chi_{alt} = (N\beta^2g^2/9k_BT)\, S(S + 1)\, F_{alt} \quad (2)$$

$$F_{alt} = \{3(1 - u_1^4u_2^2) + 4u_1(1 - u_1^2u_2^2) + 2u_2(1 + u_1)^2(1 - u_1^2) + 2u_1^2(1 - u_2^2)\} \,/\, (1 - u_1^2u_2)^2 \quad (3)$$

where $u_i = \coth(x) - 1 / x$, $x = [J_iS(S + 1)] / k_BT$, and N, β, g, and k_B have their usual meanings. If the antiferromagnetic coupling is weak or its character is ferromagnetic, the influence of zero-field splitting (zfs) must be taken into account in an analysis of the magnetic behavior at low temperatures. The bulk susceptibility of **1a** and **2a** was calculated in the 5–300 K temperature range by the combination [2-4] of zfs and the alternating chain $J_1J_1J_2$... as:

$$\chi = \chi_{zfs} \cdot F_{alt} \cdot S(S + 1)/9 \cdot 4/5 \quad (4)$$

assuming that the zfs part can be represented by [5]:

$$\chi_{zfs} = (\chi_{||} + 2\chi_{\perp}) / 3 \quad (5)$$

$$\chi_{||} = (N\beta^2g_{||}2/4k_BT)\,(1 + 9d^2) / (1 + d^2) \quad (5a)$$

$$\chi_{\perp} = (N\beta^2g_{\perp}^2/k_BT)\,[1 + 3k_BT/4D \cdot (1 - d^2)] / (1 + d^2) \quad (5b)$$

where d = exp ($-D/k_BT$) and D is the axial zfs parameter. The coefficient 4/5 in Eq. (4) ensures that for D = 0 this equation reduces to susceptibility of the alternating chain $J_1J_1J_2$ of Abu-Youssef [1]. In order to avoid overparametrization isotropic g value was assumed. The best agreement between theory and experiment was obtained for J_1 = –1.62 cm^{-1}, J_2 = 0.83 cm^{-1}, D = 52.1 cm^{-1}, g= 2.61 (R = $\sum[(\chi T)_{exp} - (\chi T)_{calc}]^2 / \sum[(\chi T)_{exp}]^2 = 3.0\cdot10^{-5}$) for **1a** and J_1 = –1.58 cm^{-1}, J_2 = 0.25 cm^{-1}, D = 43.8 cm^{-1}, g= 2.71 (R = $1.5\cdot10^{-5}$) for **2a**. The susceptibility curves resulting from the above parameters [depicted as $\mu_{eff}(T)$] are shown in Figure S25.

References

1. M. A. M. Abu-Youssef, M. Drillon, A. Escuer, M. A. S. Goher, F. A. Mautner and R. Vicente, *Inorg. Chem.*,2000, **39**, 5022.
2. C. G. Barraclough, A. K. Gregson and S. Mitra, *J. Chem. Phys.*, 1974, **60**, 962.
3. F. S. Delgado, N. Kerbellec, C. Ruiz-Pérez, J. Cano, F. Lloret and M. Julve, *Inorg. Chem.*, 2006, **45**, 1012.
4. F. Lloret, M. Julve, J. Cano, R. Ruiz-García and E. Pardo, *Inorg. Chim. Acta*, 2008, **361**, 3432.
5. R. Boča, *Struct. Bond.*, 2006, **117**, 1.

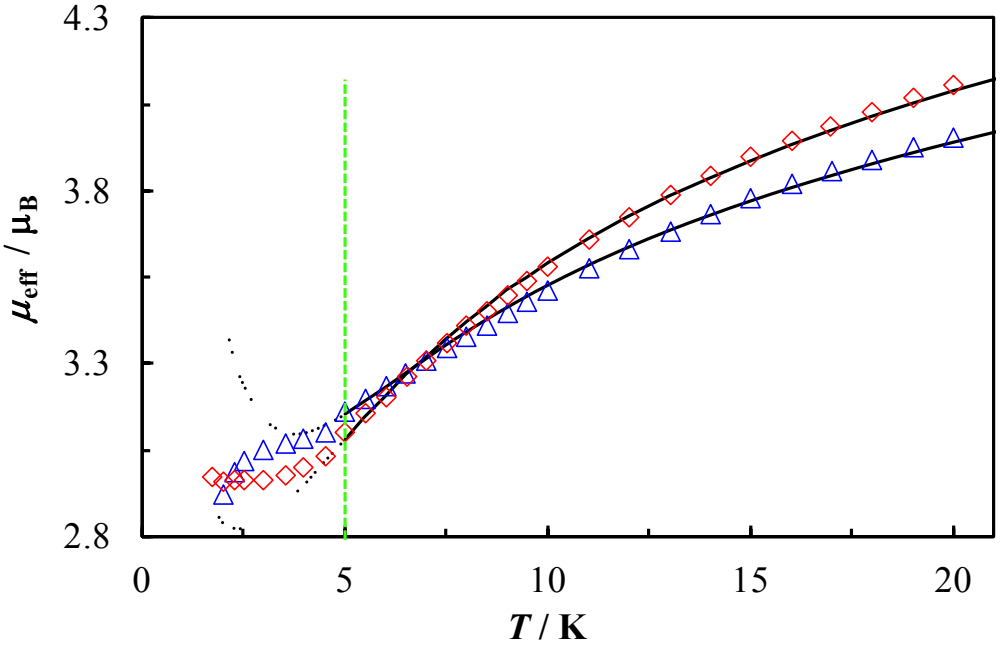

Figure S25. Temperature dependence of the effective magnetic moments of **1a** (triangles) and **2a** (diamonds) below 20 K, measured in 0.100 *T*. Solid lines show the best fit of the data according to model **B**. Data for the full temperature range are practically identical to those calculated by method **C** (Figures S24 and S25).